1D Modelling of the Venusian Planetary Interior

Srujan Vaidya (5072034), Lorenz Veithen (5075211) - Hours spent: 22h/each

May 22, 2023

1 Introduction

A deep understanding of the internal structure of planetary bodies is fundamental to the quest for clues on the origin of life and the formation of the planetary systems. From the young surface of Triton to the fascinating landscapes of Mars and the volcanoes of Venus, planetary interiors have the potential to yield crucial insights into topics ranging from the thermal behaviour of a planet, to its evolution and the creation of its atmosphere. The interior of a planetary body is the background for all numerical modelling analysis on its characteristics, ranging from gravity modelling to tidal and loading deformations. In this assignment, a preliminary 1D model of the interior of Venus is developed and validated with respect to literature.

The Venusian system has been studied in details through both observational data made from Earth, and space missions such as Venus Express and Magellan. These yielded information on properties of the planet given by [1] in Table 1[1]. Note that the Mean Moment of Inertia (MMI) is known to have a large uncertainty, as direct measurements are not possible due to the planet's slow self-rotation (243 Earth days) [2]. Furthermore, while missions have been focused on studies surrounding the atmosphere of Venus, the latter two missions had experiments aiming to study the interior of the planet. Namely, Venus Express studied the magnetic field of the planet [3] and yielded data on its surface temperature [4], and Magellan permitted to obtain gravity field and density distributions data of the planet [5].

Table 1: Observational data and parameters of Venus.

Parameters	Values
Mass [1, 6], [kg]	$4.869e24$
Equatorial radius [1, 6], [km]	6051.53
Mean density [1, 6], [kg/m^3]	5250
MMI [2], J/MR^2 [-]	0.337±0.024
Surface temperature [7], [K]	750
Surface pressure [8], [bar]	93

Despite the lack of seismology data to reveal direct clues on the internal structure of Venus, a variety of models have been proposed in literature to describe the Venusian interior. One presented by Aitta [9] makes use of the similarity between the observational parameters of Venus and Earth to postulate a similar interior structure. It is then widely believed that the Venusian interior is composed of a Silicate crust, a magnesium silicate mantle and a fluid iron rich core[2] [9, 10]. The density profile of Venus' mantle (from the crust to a pressure of 23.83 GPa) is directly derived from linear extrapolation of Earth's density profile in the transition zone. Furthermore, the planet's core is modelled using the tricritical phenomena applied to Iron. These models combined with planetary equations for pressure, gravity, and an adiabatic temperature model give rise to the results shown in Figure 1.

In a more recent study from Fienga *et al.* [11] a four layer model based on the assumption of hydrostatic equilibrium, homogeneous layers, and spherically symmetrical planet, was used. Following Aitta [9], James, Zuber, and Phillips [12], and Davis [13], the study uses the four layer model described by Table 2.

Table 2: Four layer model used by [11]. L=Lower, U=Upper.

Layers	Core	L-Mantle	U-Mantle	Crust
r [km]	3228	5332	6022	6052
$\bar{\rho}$ [kg/m^3]	9800	4850	3760	2900

Furthermore, a detailed numerical modelling study of the Venusian interior based on its chemical composition, was investigated by Shah *et al.* [14]. A large variety of compositions were investigated, for the entire uncertainty range of the MMI shown in Table 1 and for different S-contents (nominal: $X_{FeS}^{Core} = 0.08$-0.15; S-rich: $X_{FeS}^{Core} = 0.2$–0.5; S-free: $X_{FeS}^{Core} = 0$). Results could not exclude the possible existence of a solid inner core, and found that stable inner structures were only possible for MMI between 0.317 and 0.351 (upper bound for S-rich and lower bound for both S-free and nominal cases). An overview of the possible internal structures of the planet depending on the S-content considered is given by Figure 2, and the density, temperature, and pressure profiles for the nominal case, are shown in Figure 3 [14].

In this assignment, a 1D model of the radial interior structure of Venus in terms of pressure, density, gravity, temperature, and composition, is derived and implemented. First, a layered homogeneous-density model is developed to obtain preliminary pressure and gravity

[1] These numbers are considered accurate as they also match well with the up-to-date NASA fact sheet about Venus: https://nssdc.gsfc.nasa.gov/planetary/factsheet/venusfact.html [accessed on 16th May 2023].

[2] Determined through tidal responses.

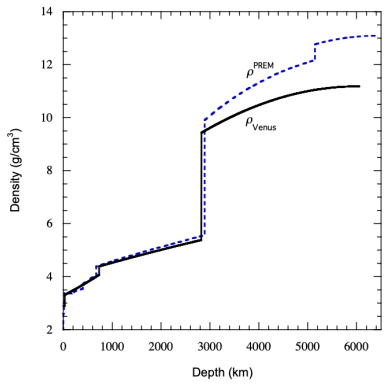

(a) Density profile in of the Venusian and Earth interior. Bold line gives values for Venus and striped line gives values for Earth.

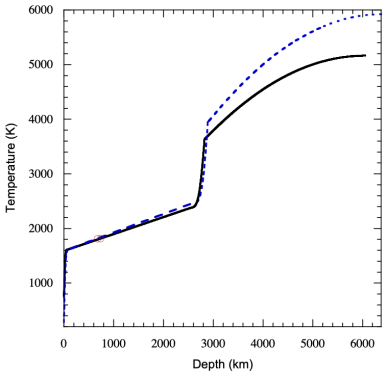

(b) Temperature profile of the Venusian interior. Bold line gives values for Venus and striped line gives values for Earth.

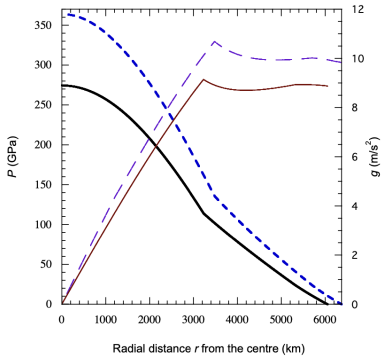

(c) Pressure and gravity profile of the Venusian interior. Bold line gives values for Venus and striped line gives values for Earth. Thinner lines refer to gravity and thicker lines refer to pressure.

Figure 1: Venusian interior according to [9].

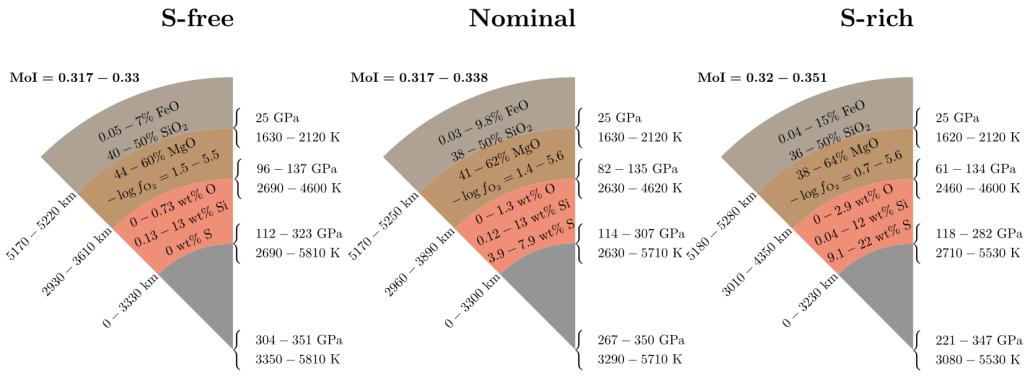

Figure 2: Possible internal structures for S-free, nominal and S-rich contents [14].

profiles. Second, first-order temperature and pressure effects are included in the model through consideration of three adiabatic thermal scenarios and iterations on the density, pressure, gravity and temperature profiles. Third, a higher fidelity model of the interior of Venus is generated using the BurnMan software [15], in order to validate the preliminary models developed.

The paper is structured in the following manner. section 2 describes the methodologies used for each of the three aforementioned models. Then, section 3 presents the key results obtained from the application of the models, including density, pressure, gravity, and temperature profiles of the 1D planet. Following, those profiles and the fit of the numerical models to the observational parameters from Table 1 are discussed in section 4. Finally, conclusions and recommendations on further work in the field are given in section 5.

2 Methodology

In this section, the methodology used in the development of the three models for the internal structure of Venus is given. For each model, four layers are considered: the crust, upper mantle, lower mantle, and core. Therefore, the possibility of an inner core presented by Shah *et al.* [14] is not considered in this work. The basic composition of the layers is given as follows: a balsatic crust as suggested by Smrekar, Davaille, and Sotin [16]; an upper mantle made of (Mg, Fe)$_2$SiO$_4$ olivine, and a lower mantle made of (Mg, Fe)SiO$_3$ perovskite and (Mg,Fe)O wuestite, as suggested by Shah *et al.* [14]; and an iron-rich core with Mg0 (5.5 wt.%) and MgSiO$_3$ (3.5 wt.%) suggested by Aitta [9].

2.1 Model 1

For the first model, a four-layer model of Venus is considered with properties given in Table 2. The density is assumed to be homogeneous throughout a layer and the coordinate system is defined from the centre with r = 0 km to the surface r = R = 6051.53 km. The pressure profile of the planet is based on the hydrostatic equilibrium relation, which depends on the gravity profile which in turn depends on the mass distribution given by the following relations:

$$dp = -\rho(r)g(r)dr \tag{1}$$

$$g(r) = \frac{GM(r)}{r^2} \tag{2}$$

$$dM = 4\pi\rho(r)r^2dr \tag{3}$$

From the density profile, the mass and gravity profiles are computed from the centre to the surface of Venus (upward integration). Following, the pressure is

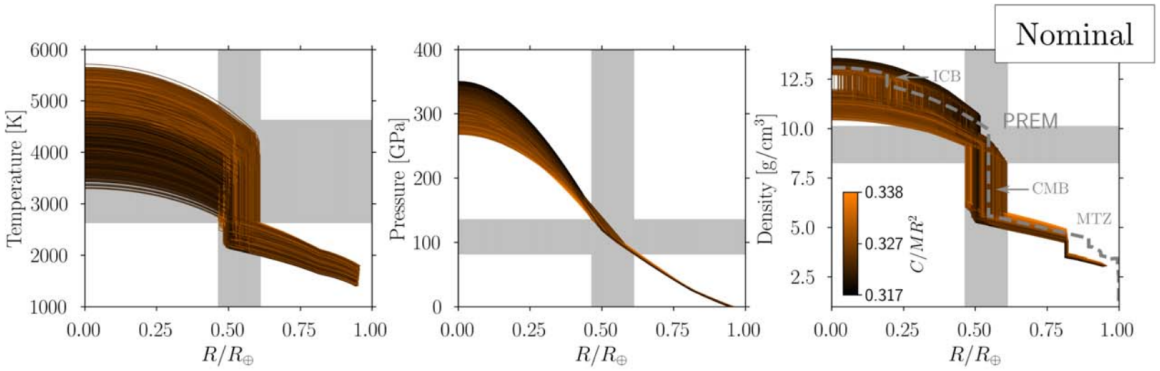

Figure 3: Density, temperature, and pressure profiles for the nominal case [14].

obtained through a downward integration from the surface to the centre with an initial surface pressure of 93 bar. The integration is done using the Forward-Euler scheme,

$$M_{n+1} = M_n + \frac{dM}{dr}\Delta r \tag{4}$$

$$p_{n+1} = p_n + \frac{dp}{dr}\Delta r \tag{5}$$

2.2 Model 2

Following, a second model taking into account the thermal environment of the planet was implemented. The density in each layer is then corrected for the temperature and pressure effects instead of letting it be homogeneous.

$$\rho(p,T) = \rho_0\left(1 - \alpha_T\Delta T + \frac{1}{K}\Delta p\right) \tag{6}$$

where ρ_0 is the reference density at the start of each layer, α_T is the thermal expansion coefficient and K is the bulk modulus of the layer. ΔT and Δp are the difference in temperature and pressure at a given point in the layer with respect to temperature and pressure at the start of the layer. A temperature profile of the planet is then required to evaluate the relationship. It is assumed that the crust of Venus is conductive (similarly to Earth's crust [17], leading to a linear temperature profile), followed by a convective upper and lower mantle and a convective core. While Aitta [9] provided some evidence for lower and upper mantle convection, the assumption of convection within the core is a model simplification (which will be revisited in Model 3). The thermal gradient in the crust was previously estimated to be very similar to Earth's, at a value of 24 K/km [18], which will be used for the first conductive layer. For the convective layers, the temperature is calculated by assuming a steady-state adiabatic profile given by,

$$\frac{dT}{dz} = \frac{\alpha g T}{C_p} \tag{7}$$

where T is a reference temperature for the layer and the values of the material properties (α, C_p) are listed in Table 3. Using this temperature profile, the density is corrected by Equation 6. With the new density profile, the mass, gravity, pressure and temperature profiles are recalculated to redo the density correction and iterated until the mass and MMI converge. With this setup, ρ_0 for each layer is tweaked until the total mass and MMI fits the observational values given in Table 1.

2.3 Model 3

The BurnMan software [15] was used for the validation of the models presented above. BurnMan is an open-source python toolkit which can be used to compute the physical and chemical properties of end-member minerals, fluids/melts, solutions, and composite assemblages [34], and permits to include a larger range of the physics at play. Similarly to the previous models, the interior was modelled as four independent layers: core, lower mantle, upper mantle, and crust. Using the Rayleigh number from Eq. (9), the dominance of conduction or convection as heat transfer mechanism for each layer is assessed:

$$\kappa = \frac{k}{\rho C_p} \tag{8}$$

$$Ra = \frac{\rho\alpha g\Delta T D^3}{\kappa\eta} \tag{9}$$

where ρ is the average density of the layer considered (the densities given in Table 2 are used), α is the thermal expansion coefficient, g is the gravitational attraction within the layer (an average value throughout the layer is used), ΔT is the change in temperature throughout the layer, D is the layer thickness, k is the thermal conductivity, C_p is the heat capacity, κ is the thermal diffusivity, and η is the dynamic viscosity. For a preliminary estimation of the Rayleigh number in each layer, the material properties shown in Table 3 are used, and the average gravity values are taken from the results of Model 1. Note, however, that the viscosity of planetary cores of Earth-like planets is subject to debate in the scientific community, with estimated values spanning about 20 orders of magnitude depending on the assumptions made [30, 31]. In this work, a molten-iron core (with no solid inner core) is assumed, leading

Table 3: Material properties of layers.

Layer	Crust	Upper Mantle	Lower Mantle	Core
Rock Material	Basalt	Olivine	Wuestite	Iron
$\boldsymbol{\alpha}$ $[\boldsymbol{K^{-1}}]$ [19, 20, 21]	-	3.5e-5	1.7e-5	4.63e-5
$\boldsymbol{C_p}$ $[\boldsymbol{Jkg^{-1}K^{-1}}]$ [22, 23, 24]	-	1713.4	817.2	835
K [GPa] [25, 26, 27, 28]	30	130	150	150
$\boldsymbol{\eta}$**[Pa s]** [29, 30, 31]	-	5e18	1e21	0.015
k $[\mathbf{W/m \cdot K}]$ [32, 33]	-	1.5	8	80.2

to a small viscosity[3]. Following, the values of ΔT are derived from the nominal case in Figure 2 (neglecting the solid inner core and using three temperature profiles: min/mean/max), the thermal gradient in the crust (24 K/km, [18]), and the surface temperature of 750 K [7]. This leads to three thermal profiles (T_1 at the boundary between the crust and upper mantle, T_2 at the boundary between upper and lower mantle, T_3 at the boundary between lower mantle and core, and T_4 is the central temperature): (1-min) $T_1 = 1458.0$ K, $T_2 = 1630$ K, $T_3 = 2630$ K, $T_4 = 3290$ K; (2-mean) $T_1 = 1458.0$ K, $T_2 = 1875$ K, $T_3 = 3625$ K, $T_4 = 4170$ K; (3-max) $T_1 = 1458.0$ K, $T_2 = 2120$ K, $T_3 = 4620$ K, $T_4 = 5710$ K. Additionally, the crust is excluded from this analysis, as strong evidence for its conductive nature exists through comparative planetology.

The Rayleigh number of each layer used in Model 3 is given in Table 4, showing that all values are above 1e6, meaning that convection is the dominant heat transfer mechanism in those layers [35][4].

Table 4: Rayleigh's number of the upper mantle, lower mantle, and core of Venus.

Layer	Profile 1	Profile 2	Profile 3
Upper Mantle	5.79e9	1.40e10	2.23e10
Lower Mantle	3.24e6	5.66e6	8.09e6
Core	3.00e27	2.48e27	4.96e+27

Based on the classification of conductive and convective layers, a complete model of the planet was setup using BurnMan, with the layer thicknesses given in Table 2. The basic composition of each layer was approximated using the mineralogy database provided with the software, based on [9, 14, 16]:

1. **Core**: liquid iron modified to contain impurities composed of S, O, and Si.
2. **Lower mantle**: Mg and Fe perovskite [36], and wuestite [37].
3. **Upper mantle**: Mg - Fe Olivine [38].
4. **Crust** (basalt): Mg - Fe Olivine [38], orthopyroxene [38], clinopyroxene [38], and periclase [37].

The molar fractions of each material, and their weight fractions in the layer composition, were iterated upon to better fit the observations from Table 1. Adiabatic heat transfer modes were implemented in the mantles and core, and the temperature profile in the crust was assumed linear with a thermal gradient of 24 K/km [18] (conduction). Furthermore, Boundary Layer Perturbations (BLP) were added to both the lower and upper mantles with their respective Rayleigh numbers and zero boundary layer ratios (to limit the number of parameters to vary). Additionally, the temperature change on the BLP was varied to better fit the observational parameters.

[3]However, the addition of impurities would result in a higher viscosity, meaning that the value used in an underestimate.

[4]Under the assumption of a liquid iron core.

3 Results

In this section, key results for each model are presented. All models were tuned to better fit the mass and mean moment of inertia of Venus given in Table 1, and for the latter the values were tuned towards the centre value of 0.337([5]).

The density, gravity and pressure profiles for the four-layer homogeneous density model are given in Figure 4. Additionally, the obtained mass and mean moment of inertia of the planet shown in Table 5 fit the observations with an accuracy of 0.009% and 2.5%[6] respectively.

Following, the density, temperature, pressure, and gravity profiles for the temperature and pressure corrected four-layer model are shown in Figure 5. Those were computed for three different values of the reference temperature in Eq. (7): 1400 K, 1900 K, 2400 K. Furthermore, the obtained mass and mean moment of inertia of the planet shown in Table 5 fit the observations with an accuracy of 0.5% and 0.4%[7] respectively.

The profiles obtained using the third model (built in BurnMan) are given by Figure 6. The obtained planet mass and mean moment of inertia shown in Table 5, which fit the observations with an accuracy of 0.0008% and 1.6%[8] respectively. Those results were obtained using the following layer compositions:

1. **Core**: Fe (92%), S (6%), O (0.5%), and Si (6.5%); mass fractions)
2. **Lower mantle**: Mg (30%) and Fe (40%) perovskite [36], and wuestite (30%) [37]; mass fractions.
3. **Upper mantle**: Mg (92%) - Fe (8%) Olivine [38]; molar fractions.

[5]although results within the uncertainty range are considered accurate.

[6]Within the uncertainty range.

[7]Within the uncertainty range.

[8]Within the uncertainty range.

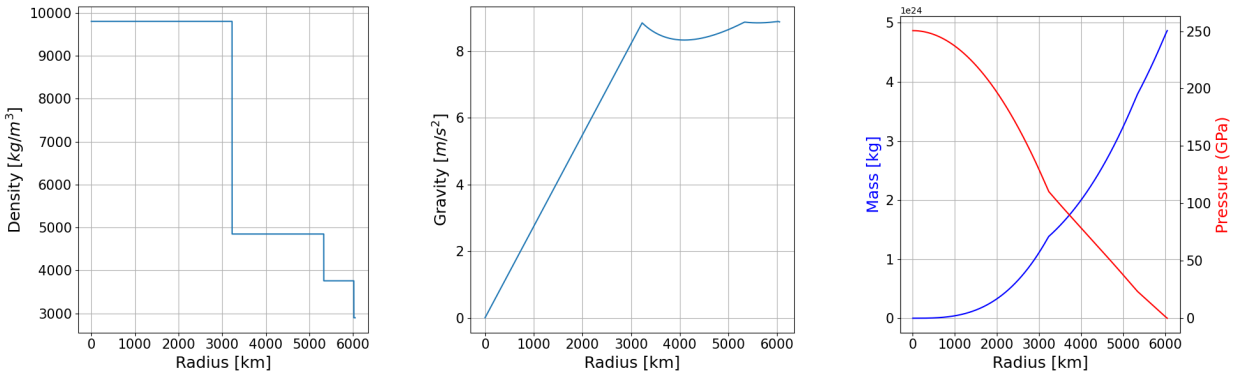

(a) Density profile of the Venusian and Earth interior for Model 1.

(b) Gravity profile of the Venusian interior for Model 1

(c) Pressure and Mass profile of the Venusian interior for Model 1.

Figure 4: Venusian interior according to Model 1.

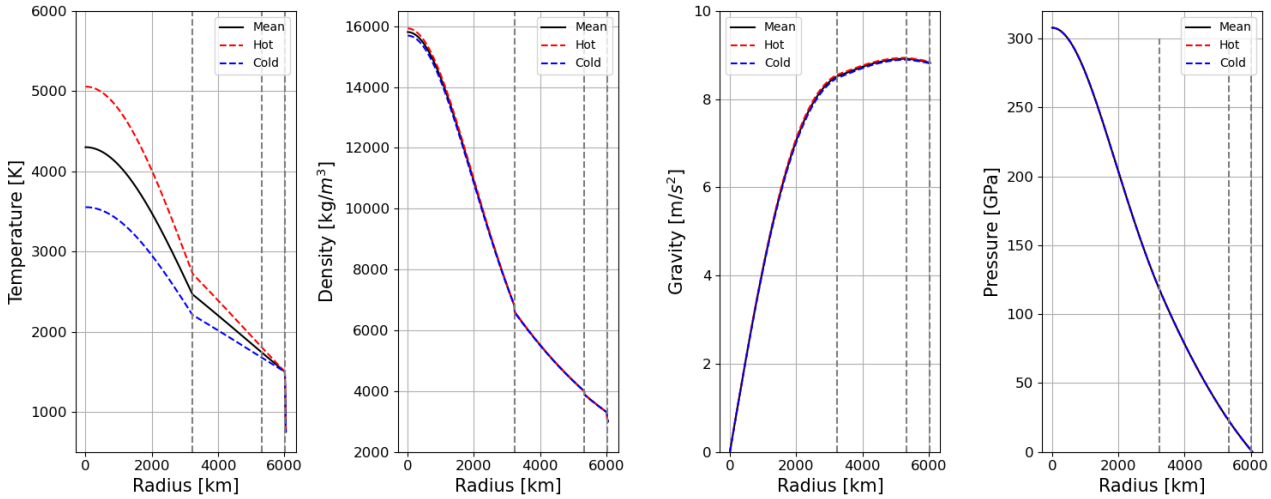

Figure 5: Temperature, density, gravity, and pressure profiles using an adiabatic profile for convective layers with three different average temperatures (Mean = 1900 K, Hot = 2400 K, and Cold = 1400 K), according to Model 2.

4. **Crust** (basalt): Mg - Fe Olivine [38] (Mg 67%, Fe 33% molar fractions), orthopyroxene (molar fractions 0.1, 0.1, 0.1, 0.7) [38], clinopyroxene (molar fractions 0.1, 0.1, 0.1, 0.1, 0.6) [38], and periclase [37]; with mass fractions of 20-20-20-40% respectively.

In combination with a temperature change of 1250 K at the boundary between the core and lower mantle.

4 Discussion

Comparing the profiles in Figure 4 to the results obtained by Aitta [9] in Figure 1, it is clear that despite the simplicity of the first model, good first order estimates of the gravity and pressure profiles are obtained. That is, similar shapes and surface values result, while fitting the mass and MMI observations reasonably well. However, model 1 does not provide temperature estimates, and results in a very sharp and discontinuous density profile, which is considered unphysical.

Following, Model 2 results in a lower accuracy of the mass observations, but seems to better fit the MMI data (however, the latter has a much larger uncertainty). Furthermore, the profiles shown in Figure 5 are significantly different from the results obtained by Aitta [9] and Shah *et al.* [14]: reaching much higher densities at the core and being mostly continuous, a temperature profile without sharp rise at the boundary between the core and lower mantle[9], and the gravity profile is mostly monotonous. However, the model results in central temperatures and pressures which fall within the range suggested by Shah *et al.* [14] in Figure 2, and shows similar average densities as Model 1 (see Table 6).

Model 3 provides the best estimate for the mass observation, while still keeping the MMI within the uncertainty range (and within 1.6% of the centre value). The model used the most general modelling of physics and permitted to gain some understanding of the true composition of each layer. Similarly to Model 2, Model 3 results in similar average densities to Model 1 (which was suggested by Fienga *et al.* [11]) on each layer. Furthermore, comparing the profiles produced by Aitta [9] and Model 3 in Figure 6, a similar behaviour in the gravity and density curves is found, while matching the

[9]Which could be expected based on the similar physics in Earth's interior.

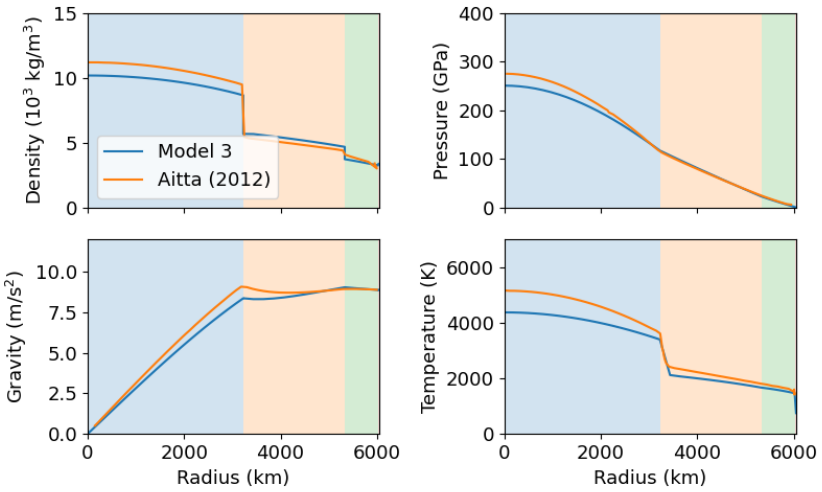

Figure 6: Density, pressure, gravity and temperature profiles according to Model 3, and compared to the model presented by Aitta [9]. The curves presented by Shah *et al.* [14] were not included for readability.

Table 5: Mass and mean moment of inertia obtained (after tuning) for each model.

# Model	Mass, [kg]	MMI, [-]
Observed	4.869e24	0.337±0.024
Model 1	4.8686e24	0.3456
Model 2	4.8417e24	0.3357
Model 3	4.869e24	0.3425

Table 6: The average density $[kg/m^3]$ of each layer for the different models.

Layer	Model 1	Model 2	Model 3
Crust	2900	3051	3358
Upper Mantle	3760	3589	3483
Lower Mantle	4850	5207	5244
Core	9800	11990	9707

behaviour suggested in Figure 3. However, the profiles seem to diverge from each other at the core, showing that different modelling assumptions were made (composition, heat transfer mechanism, etc.). Particularly, the assumption of convection in the fully fluid core is a modelling simplification as convection is only possible if a growing solid inner core is present [9] (which may have been modelled differently by Aitta [9]). This difference results in a smaller density, pressure and temperature at the core of the planet of Model 3 compared to the reference. Additionally, the latter is on the lower side compared to the suggested realistic range by Shah *et al.* [14] in Figure 3 for nominal S-contents.

All models fit the mass and mean moment of inertia with a reasonable degree of accuracy ($\sim 2.5\%$ at most). However, the MMI has a much larger uncertainty, meaning that a better match of the numerical model with the mass is desired, and predicted values of MMI within the uncertainty range are acceptable. In this respect, Model 3 results in a higher accuracy while considering a wider range of physics phenomena, and matching the rest of the literature to a reasonable extent (giving confidence in the model). Model 3 is then considered to be the most promising model produced in this work.

5 Conclusion

Three models with increasing complexity were produced, providing insights into the density, gravity, pressure, and temperature profiles, as well as indications on the possible material composition of the layers. The third model, developed in BurnMan, was found to be the most promising, and yielded mass and mean moment of inertia estimates of the planet of 4.869e24 kg and 0.3425 respectively. Those estimates match the mass observations with an accuracy of 0.0008% and fall in the uncertainty range for the MMI. The model predicts a central temperature and pressure of 4372 K and 250 GPa respectively, which are in the same order of magnitude as previously suggested in literature. Improvements on the developments and analysis performed in this work include:

1. Impact of the thermal gradient in the Venusian crust, which was assumed at 24 K/km based on [18]. Iterating on this value may lead to even more accurate fit of the observation data.
2. The convection in the molten core is only possible if some growing solid inner core exists [9], meaning that the use of an adiabatic temperature profile, and convection within the core is a model simplification. Reconsideration of this assumption is necessary to improve the reliability of the third model presented.
3. The accuracy of the models, and the confidence which can be put into them, is limited by the available data on Venus interior. With future missions, such as EnVision, more observations will become available to permit further assessment of the Venusian internal structure.

Bibliography

[1] V. N. Zharkov. "Models of the internal structure of Venus". In: *The moon and the planets* 29.2 (1983), pp. 139–175. DOI: 10.1007/BF00928322. URL: https://doi.org/10.1007/BF00928322.

[2] Jean-Luc Margot *et al.* "Spin state and moment of inertia of Venus". In: *Nature Astronomy* 5.7 (2021), pp. 676–683. DOI: 10.1038/s41550-021-01339-7. URL: https://doi.org/10.1038/s41550-021-01339-7.

[3] T.L. Zhang *et al.* "Initial Venus Express magnetic field observations of the Venus bow shock location at solar minimum". In: *Planetary and Space Science* 56.6 (2008). Mars Express/Venus Express, pp. 785–789. ISSN: 0032-0633. DOI: https://doi.org/10.1016/j.pss.2007.09.012. URL: https://www.sciencedirect.com/science/article/pii/S0032063307003777.

[4] *VIRTIS: The Visible and Infrared Thermal Imaging Spectrometer*. Vol. 1295. ESA Special Publication. Dec. 2007.

[5] Robert R. Herrick and Roger J. Phillips. "Geological correlations with the interior density structure of Venus". In: *Journal of Geophysical Research: Planets* 97.E10 (1992), pp. 16017–16034. DOI: https://doi.org/10.1029/92JE01498. eprint: https://agupubs.onlinelibrary.wiley.com/doi/pdf/10.1029/92JE01498. URL: https://agupubs.onlinelibrary.wiley.com/doi/abs/10.1029/92JE01498.

[6] V. N. Zharkov, T. V. Gudkova, and A. Nikol'skii. "On Parameters of the Earth-Like Model of Venus". In: *Solar System Research* 53.1 (2019), pp. 1–4. DOI: 10.1134/S0038094618060084. URL: https://doi.org/10.1134/S0038094618060084.

[7] F. Westall *et al.* "The Habitability of Venus". In: *Space Science Reviews* 219.2 (2023), p. 17. DOI: 10.1007/s11214-023-00960-4. URL: https://doi.org/10.1007/s11214-023-00960-4.

[8] Alexander T Basilevsky and James W Head. "The surface of Venus". In: *Reports on Progress in Physics* 66.10 (2003), p. 1699. DOI: 10.1088/0034-4885/66/10/R04. URL: https://dx.doi.org/10.1088/0034-4885/66/10/R04.

[9] A. Aitta. "Venus' internal structure, temperature and core composition". In: *Icarus* 218.2 (2012), pp. 967–974. ISSN: 0019-1035. DOI: https://doi.org/10.1016/j.icarus.2012.01.007. URL: https://www.sciencedirect.com/science/article/pii/S001910351200022X.

[10] A. S. Konopliv and C. F. Yoder. "Venusian k2 tidal Love number from Magellan and PVO tracking data". In: *Geophysical Research Letters* 23.14 (1996), pp. 1857–1860. DOI: https://doi.org/10.1029/96GL01589. eprint: https://agupubs.onlinelibrary.wiley.com/doi/pdf/10.1029/96GL01589. URL: https://agupubs.onlinelibrary.wiley.com/doi/abs/10.1029/96GL01589.

[11] Agnes Fienga *et al.* "Exploring Venus internal structure and its tidal response". In: *EPSC-DPS Joint Meeting 2019*. Vol. 2019. Sept. 2019, EPSC-DPS2019-1939, EPSC-DPS2019–1939.

[12] P. B. James, M. T. Zuber, and R. J. Phillips. "Geoid to Topography Ratios on Venus and Implications for Crustal Thickness". In: *41st Annual Lunar and Planetary Science Conference*. Lunar and Planetary Science Conference. Mar. 2010, p. 2663.

[13] Andrew M Davis. *Meteorites, Comets, and Planets: Treatise on Geochemistry, Volume 1*. Vol. 1. Elsevier, 2005.

[14] Oliver Shah *et al.* "Possible Chemical Composition And Interior Structure Models Of Venus Inferred From Numerical Modelling". In: *The Astrophysical Journal* 926.2 (2022), p. 217. DOI: 10.3847/1538-4357/ac410d. URL: https://dx.doi.org/10.3847/1538-4357/ac410d.

[15] Sanne Cottaar *et al.* "BurnMan: A lower mantle mineral physics toolkit". In: *Geochemistry, Geophysics, Geosystems* 15.4 (2014), pp. 1164–1179. DOI: https://doi.org/10.1002/2013GC005122. eprint: https://agupubs.onlinelibrary.wiley.com/doi/pdf/10.1002/2013GC005122. URL: https://agupubs.onlinelibrary.wiley.com/doi/abs/10.1002/2013GC005122.

[16] Suzanne E. Smrekar, Anne Davaille, and Christophe Sotin. "Venus Interior Structure and Dynamics". In: *Space Science Reviews* 214.5 (2018), p. 88. DOI: 10.1007/s11214-018-0518-1. URL: https://doi.org/10.1007/s11214-018-0518-1.

[17] Christoph Clauser. "Heat Transport Processes in the Earth's Crust". In: *Surveys in Geophysics* 30.3 (2009), pp. 163–191. DOI: 10.1007/s10712-009-9058-2. URL: https://doi.org/10.1007/s10712-009-9058-2.

[18] Sean C. Solomon and James W. Head. "Mechanisms for lithospheric heat transport on Venus: Implications for tectonic style and volcanism". In: *Journal of Geophysical Research: Solid Earth* 87.B11 (1982), pp. 9236–9246. DOI: https://doi.org/10.1029/JB087iB11p09236. eprint: https://agupubs.onlinelibrary.wiley.com/doi/pdf/10.1029/JB087iB11p09236. URL: https://agupubs.onlinelibrary.wiley.com/doi/abs/10.1029/JB087iB11p09236.

[19] Joseph Smyth, Steven Jacobsen, and Robert Hazen. "Comparative Crystal Chemistry of Orthosilicate Minerals". In: *Reviews in Mineralogy and Geochemistry* 41 (June 2000). DOI: 10.2138/rmg.2000.41.7.

[20] Mikako Takeda *et al.* "Physical Properties of Iron-Oxide Scales on Si-Containing Steels at High Temperature". In: *Materials Transactions - MATER TRANS* 50 (Sept. 2009), pp. 2242–2246. DOI: 10.2320/matertrans.M2009097.

[21] Yurii Kozlovskii and Sergei Stankus. "The linear thermal expansion coefficient of iron in the temperature range of 130–1180 K". In: *Journal of Physics: Conference Series* 1382 (Nov. 2019), p. 012181. DOI: 10.1088/1742-6596/1382/1/012181.

[22] Fredrik Grønvold *et al.* "Heat capacities of the wüstites Fe0.9379O and Fe0.9254O at temperatures T from 5 K to 350 K. Thermodynamics of the reactions: xFe(s) + (1/4)Fe3O4(s) = Fe0.7500+xO(s) = Fe1-yO(s) at T 850 K, and properties of Fe1-yO(s) to T = 1000 K. Thermodynamics of formation of wüstite". In: *The Journal of Chemical Thermodynamics* 25.9 (1993), pp. 1089–1117. ISSN: 0021-9614. DOI: https://doi.org/10.1006/jcht.1993.1107. URL: https://www.sciencedirect.com/science/article/pii/S0021961483711079.

[23] Richard A Robie, Bruce S Hemingway, and Humihiko Takei. "Heat capacities and entropies of Mg2SiO4, Mn2SiO4, and Co2SiO4 between 5 and 380 K". In: *American Mineralogist* 67.5-6 (1982), pp. 470–482.

[24] Pramond D Desai. "Thermodynamic properties of iron and silicon". In: *Journal of physical and chemical reference data* 15.3 (1986), pp. 967–983.

[25] Debanjan Guha Roy, Vikram Vishal, and Trilok Nath Singh. "Effect of carbon dioxide sequestration on the mechanical properties of Deccan basalt". In: *Environmental Earth Sciences* 75 (2016), pp. 1–13.

[26] Frederic Bejina *et al.* "Bulk modulus of Fe-rich olivines corrected for non-hydrostaticity". In: *Comptes Rendus Geoscience* 351.2-3 (2019), pp. 86–94.

[27] A Rajabpour, L Seidabadi, and M Soltanpour. "Calculating the bulk modulus of iron and steel using equilibrium molecular dynamics simulation". In: *Procedia Materials Science* 11 (2015), pp. 391–396.

[28] Ming Liu and Lin-gun Liu. "Bulk moduli of wüstite and periclase: a comparative study". In: *Physics of the earth and planetary interiors* 45.3 (1987), pp. 273–279.

[29] V. S. Solomatov and L.-N. Moresi. "Scaling of time-dependent stagnant lid convection: Application to small-scale convection on Earth and other terrestrial planets". In: *Journal of Geophysical Research: Solid Earth* 105.B9 (2000), pp. 21795–21817. DOI: https://doi.org/10.1029/2000JB900197. eprint: https://agupubs.onlinelibrary.wiley.com/doi/pdf/10.1029/2000JB900197. URL: https://agupubs.onlinelibrary.wiley.com/doi/abs/10.1029/2000JB900197.

[30] Christelle Saliby *et al.* "Viscosity contrasts in the Venus mantle from tidal deformations". In: *Planetary and Space Science* 231 (2023), p. 105677. ISSN: 0032-0633. DOI: https://doi.org/10.1016/j.pss.2023.105677. URL: https://www.sciencedirect.com/science/article/pii/S0032063323000466.

[31] Gilles Wijs *et al.* "The viscosity of liquid iron under Earth's core conditions". In: *Nature* 392 (Apr. 1998), pp. 805–807. DOI: 10.1038/33905.

[32] Mikako Takeda *et al.* "Physical Properties of Iron-Oxide Scales on Si-Containing Steels at High Temperature". In: *Materials Transactions - MATER TRANS* 50 (Sept. 2009), pp. 2242–2246. DOI: 10.2320/matertrans.M2009097.

[33] Werner Martienssen and Hans Warlimont. *Springer handbook of condensed matter and materials data*. Vol. 1. Springer, 2005.

[34] R. Myhill *et al. Computational Infrastructure for Geodynamics*. Version Burnman v1.1.0. 2022. DOI: https://doi.org/10.5281/zenodo.7080174.

[35] U. Madanan and R. J. Goldstein. "High-Rayleigh-number thermal convection of compressed gases in inclined rectangular enclosures". In: *Physics of Fluids* 32.1 (Jan. 2020). 017103. ISSN: 1070-6631. DOI: 10.1063/1.5134820. eprint: https://pubs.aip.org/aip/pof/article-pdf/doi/10.1063/1.5134820/15806648/017103_1_online.pdf. URL: https://doi.org/10.1063/1.5134820.

[36] Motohiko Murakami *et al.* "A perovskitic lower mantle inferred from high-pressure, high-temperature sound velocity data". In: *Nature* 485.7396 (2012), pp. 90–94. DOI: 10.1038/nature11004. URL: https://doi.org/10.1038/nature11004.

[37] J. Matas *et al.* "On the bulk composition of the lower mantle: predictions and limitations from generalized inversion of radial seismic profiles". In: *Geophysical Journal International* 170.2 (2007), pp. 764–780. DOI: https://doi.org/10.1111/j.1365-246X.2007.03454.x. eprint: https://onlinelibrary.wiley.com/doi/pdf/10.1111/j.1365-246X.2007.03454.x. URL: https://onlinelibrary.wiley.com/doi/abs/10.1111/j.1365-246X.2007.03454.x.

[38] Lars Stixrude and Carolina Lithgow-Bertelloni. "Thermodynamics of mantle minerals – II. Phase equilibria". In: *Geophysical Journal International* 184.3 (2011), pp. 1180–1213. DOI: https://doi.org/10.1111/j.1365-246X.2010.04890.x. eprint: https://onlinelibrary.wiley.com/doi/pdf/10.1111/j.1365-246X.2010.04890.x. URL: https://onlinelibrary.wiley.com/doi/abs/10.1111/j.1365-246X.2010.04890.x.